Complexity Project
The Oslo Model

Benjamin Richards

17th February 2023

Abstract: One of the simplest models to exhibit scale-free behaviour, known as criticality, is the Oslo model, first proposed in the late 90s. As many natural systems also exhibit such behaviour, such as earthquakes and rainfall, there is a great amount that can be learnt from studying such systems. This investigation sought to gain insights into self-organised criticality, where criticality is the attractor of the dynamics of a system, by analysing the pile heights and avalanche distributions of the Oslo model. Pile height was analysed, including cross-over time, corrections to scaling and standard deviation on the mean pile height, culminating in a data collapse revealing common behaviour across system sizes. Avalanche probability distribution was also analysed using the finite scaling ansatz and a subsequent data collapse. Values for the avalanche dimension, D, were found separately from the data collapse and from moment analysis to be 2.19 ± 0.01 and 2.21 ± 0.01 respectively, and for the avalanche-size exponent, τ_s, as 1.56 ± 0.01 and 1.55 ± 0.03, respectively. These values are each within two standard deviations of the other, indicating reasonable agreement.

Word count: 2,434 words in report (excluding front page, figure captions, table captions, acknowledgement and bibliography).

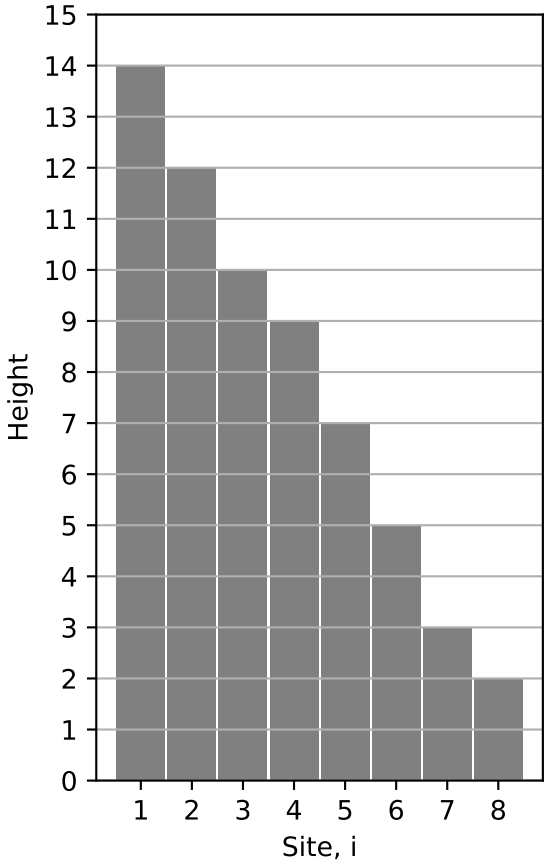

Figure 1: A plot of a system with size $L = 8$, used to check that the system is performing as expected under different conditions.

1 Introduction

There are many systems in nature, including earthquakes, rainfall and atrial fibrillation, that display scale-free behaviour, i.e. certain observables have no characteristic scale when at some phase transition, known as criticality [1]. Self-organized criticality is when criticality is an attractor of a system's dynamics, without external tuning, as first outlined by Bak, Tang and Wiesenfeld [2]. One of the simplest models that exhibits self-organised criticality is the Olso model [1], and its insights can be applied to more complex systems.

Our aim is to investigate self-organised criticality through analysis of the pile height and avalanche distribution of the Oslo model.

2 Implementation

An implementation of the Oslo model was written in Python, following the standard algorithm of initialisation, driving, relaxation and iteration. A pointer was utilised to scan through the sites, relaxing sites until an avalanche had ceased, reducing the number of sites checked.

To verify the model's accuracy, unit and end-to-end tests were conducted. A plotting method was added for visual inspection of initialisation, driving, and pile growth, Fig. 1. Threshold probability could be changed arbitrarily to make the model deterministic, allowing for 31 tests verifying class method output, tests on relaxation and statistical tests on threshold distribution.

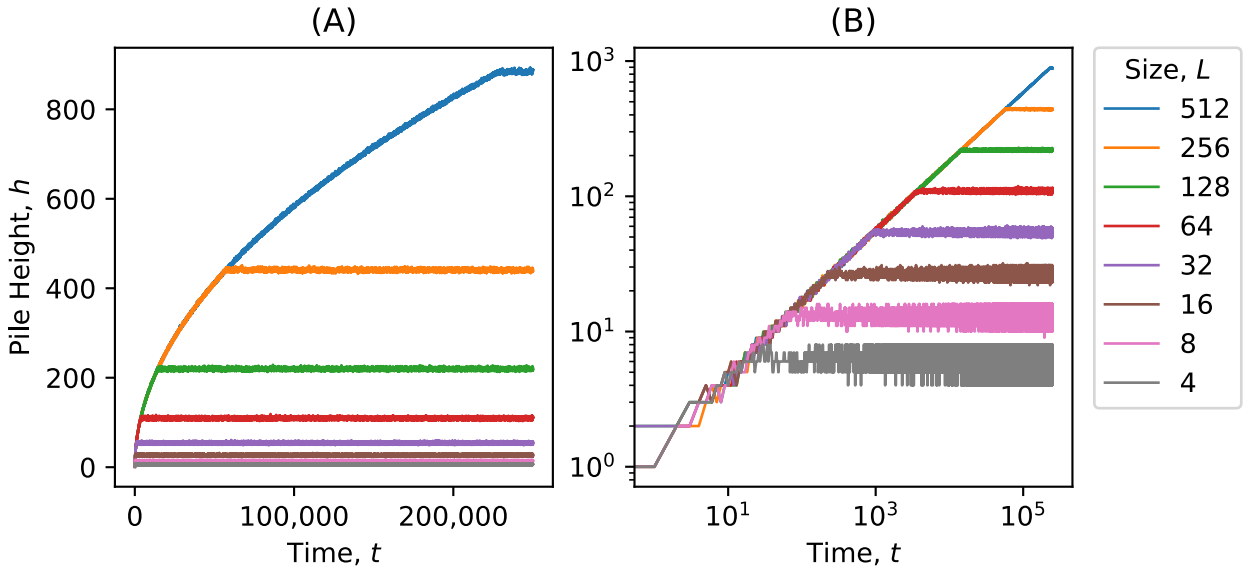

Figure 2: Height as a function of time plotted on linear-linear (A) and log-log (B) axes, for systems of various sizes, L. Each system has a transient growth phase followed by steady-state. In (B), transient phase height follows a power law and steady-state heights are evenly spaced, indicating a linear relationship between steady-state height and system size L, which changes by a factor of 2 between measured system sizes. Small systems exhibit noise from the discretisation of pile height.

3 Pile Height Investigation

First, we examine the total pile height, which can be obtained from the gradients as:

$$h(t; L) = \sum_{i=1}^{L} z_i(t), \tag{1}$$

where h is a function of t, the time measured in number of grains added to the system and L, the length of the system, and where z_i is the gradient at position i.

3.1 Pile Height as a Function of Time

The simplest way to study pile height is to analyse its dependence on time, t, for different system sizes.

Plotting pile height against time for system lengths between 4 and 512, Fig. 2, a transient growth phase initially occurs due to no grains leaving the system. Therefore, no transient gradient configurations are visited twice for a given instance. The power-law growth rate is the same for all systems, as seen in Fig. 2 (B).

This is followed by steady-state where pile height remains constant, on average, as net grain flux becomes zero. Gradient configurations thus become recurrent and accessible again at later times. The even spacing in Fig. 2 (B) shows linear proportionality between steady-state height and system size, which varies by a factor of 2 between systems.

3.2 Crossover Time as a Function of System Size

Next, we investigate the cross-over time: the number of grains in the system before an added grain causes at least one grain to leave the system. For each system size, a mean value was

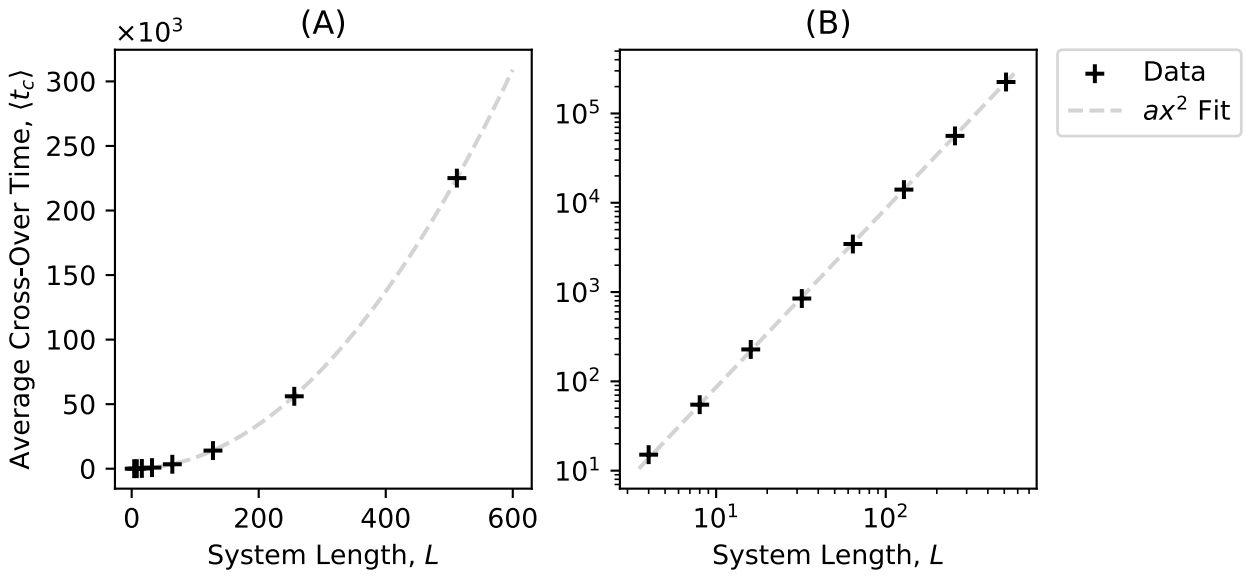

Figure 3: Cross over times for various system sizes, on linear-linear (A) and log-log (B) axes, with a fit of ax^2 matching the data well. Errors were not added since they would be too small to see, ranging from 0.4 for $L = 4$ to 442 for $L = 512$.

calculated over 10 repetitions.

Plotting average cross-over time against system size, Fig. 3, reveals that cross-over time scales with system size squared. Fitting the function ax^2 yields a proportionality constant of 0.8587 ± 0.0006, matching the data well.

3.3 Theoretical Scaling Arguments

A site's gradient is determined by the system mechanics and the site's environment, i.e. the gradients of nearby sites. System mechanics do not change with system size, but edge effects change a site's environment, causing corrections to scaling. For large systems, edge effects eventually become irrelevant, making the average gradient independent of system size.

If average gradient is independent of system size for $L \gg 1$, average steady-state pile height scales linearly with system size. Similarly, cross-over time corresponds to the area of the triangular pile, thus scaling with the square of the system size, as seen in Fig. 3.

3.4 Pile Height Data Collapse

To reduce the noise seen in Fig. 2 (B), we can measure average pile height, defined as

$$\tilde{h}(t; L) = \frac{1}{M} \sum_{j=1}^{M} h_j(t; L), \tag{2}$$

for M instances of h, where h_j is the pile height of instance j.

To collapse the data in Fig. 2 onto a single function, based on section 3.3, we predict that pile height can be expressed as

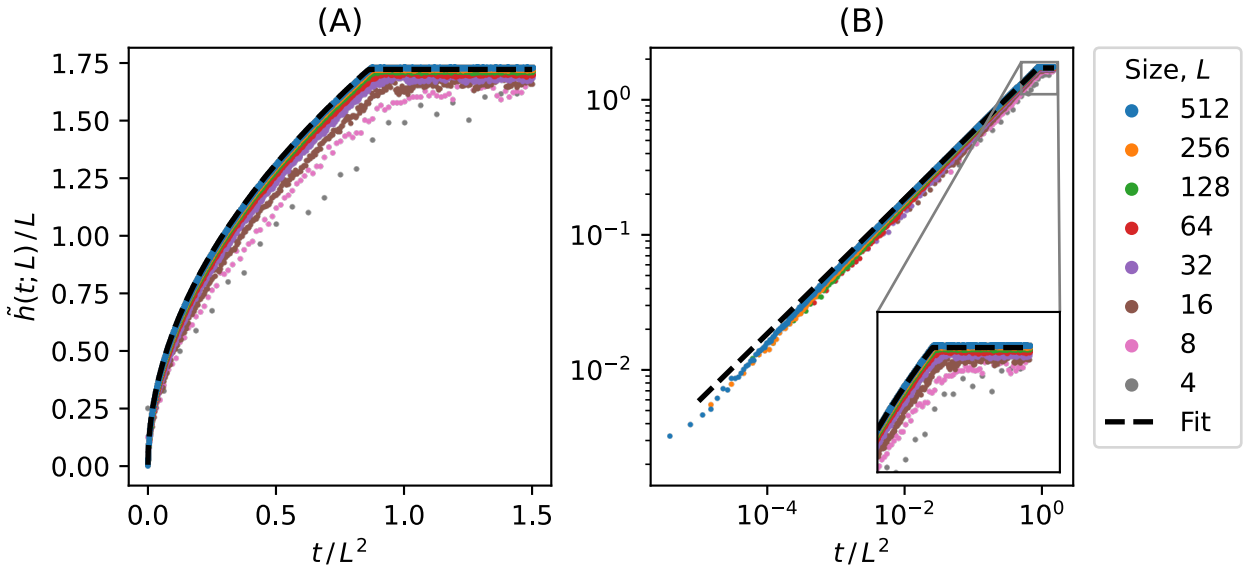

Figure 4: A data collapse of average pile height $\tilde{h}$ over 20 repetitions as a function of system size, L, and time. t, plotted on linear-linear (A) and log-log axes (B), together with a fit of the predicted form of the scaling function to the $L = 512$ data. This clearly shows the transient and steady-state phases of the scaling function, as well as verifying its predicted form.

$$\tilde{h}(t;L) = L\,\mathcal{F}(t/L^2), \tag{3}$$

$$\therefore \quad \frac{\tilde{h}(t;L)}{L} = \mathcal{F}(t/L^2), \tag{4}$$

where $\mathcal{F}$ is some scaling function. Since steady-state height scales with L, $\mathcal{F}$ must be multiplied by L to align the data vertically, in Fig. 2, and as cross-over time scales with L^2, $\mathcal{F} = \mathcal{F}(t/L^2)$ to align the data horizontally. According to equation 4, plotting $\tilde{h}/L$ against t/L^2 leads to a data collapse onto $\mathcal{F}$, the scaling function, Fig. 4.

As predicted, we find the data collapses to a single function, with corrections to scaling. From Fig. 4, we find $\mathcal{F} \to 0$ as $t/L^2 \to 0$ as expected of the transient phase, and that $\mathcal{F}$ tends to a constant value for large values of t/L^2, as expected of steady-state.

To find $\mathcal{F}(x)$, we use the results of section 3.3 to conclude

$$\mathcal{F}(x > x_c) = \frac{\tilde{h}(t > t_c\,; L)}{L} = a, \tag{5}$$

where x_c is the argument of $\mathcal{F}$ at the crossover point, and a is average gradient.

In the transient, from section 3.3, we find that

$$[h]t = \frac{1}{2} \times \text{base} \times \text{height} = \frac{\tilde{h}^2}{2a} \tag{6}$$

$$\therefore \quad \mathcal{F}(t/L^2) = \frac{\tilde{h}}{L} = \frac{\sqrt{2at}}{L} = \sqrt{2a\frac{t}{L^2}}, \tag{7}$$

equating equations 5 and 7 to find the cross-over point

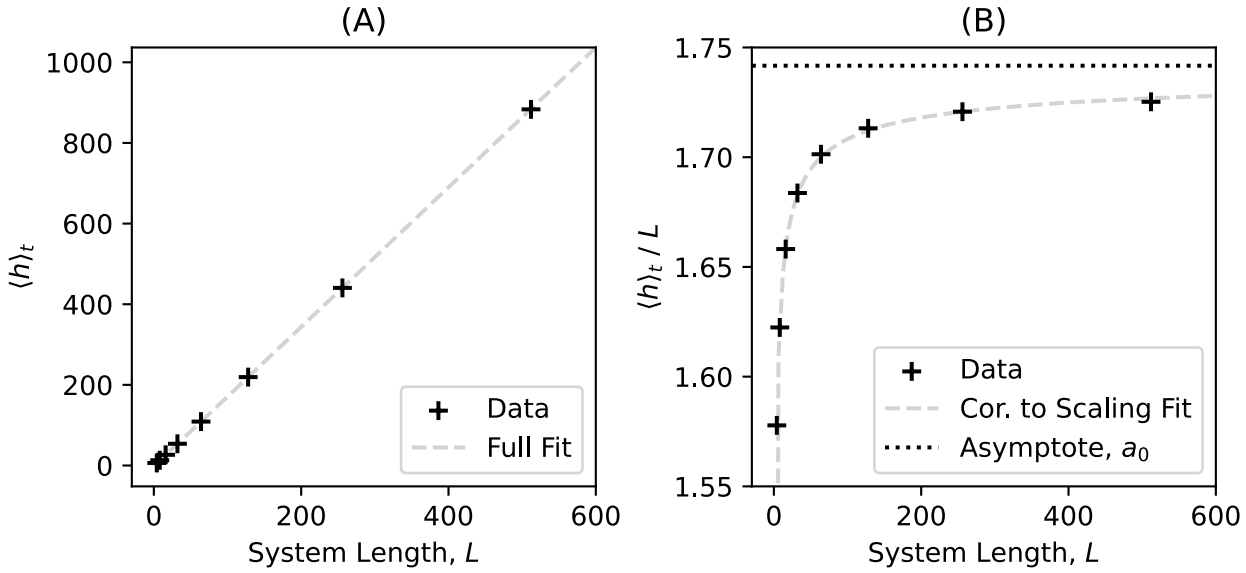

Figure 5: Time averaged pile height against system length, together with the average height scaling relation including corrections to scaling terms (A) and the average height with leading order removed against system length, showing the corrections to scaling, and the asymptotic average gradient, a_0 (B). Errors were not added to either plot, since they would be too small to see, with values for plot (A) ranging from 8.4×10^{-4} for $L = 4$ to 2.6×10^{-3} for $L = 512$. The processed data shown in (B) were used in a multi-parameter curve fit to find the corrections to scaling parameters, which were then plotted in Figure (A) for verification against the raw data.

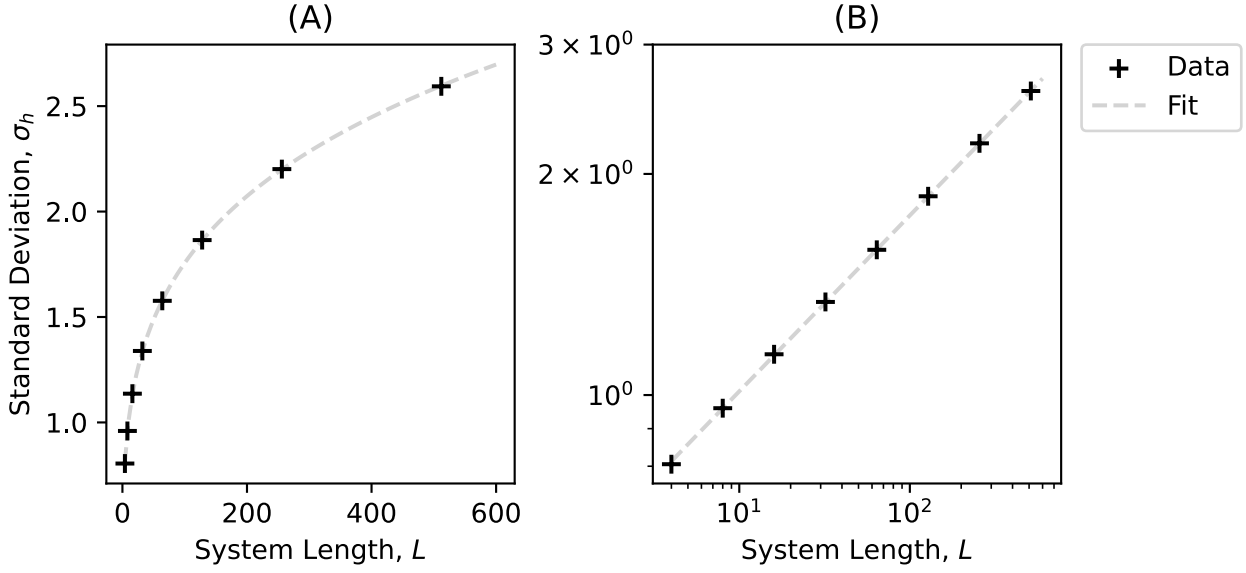

Figure 6: Standard deviation of time-averaged pile height against system length on linear-linear (A) and log-log (B) axes, together with a power law fit which agrees very well with the data. Errors were not added to plots, since they would be too small to see, with values ranging from 5.7×10^{-4} for $L = 4$ to 1.8×10^{-3} for $L = 512$.

$$\mathcal{F}(x_c) = a = \sqrt{2ax_c} \tag{8}$$

$$\therefore\ x_c = \frac{a}{2}. \tag{9}$$

which gives the full scaling function to be

$$\mathcal{F}(x) = \begin{cases} (2ax)^{1/2} & x \leq \frac{a}{2} \\ a & x \geq \frac{a}{2} \end{cases} \tag{10}$$

Since $\mathcal{F}(x)$ has a single parameter, a, we can fit it to the data. From Fig. 4 we find small systems deviate from the data collapse due to corrections to scaling. Fitting equation 10 to the largest system size $L = 512$, Fig. 4, results in good agreement, validating the equation's form.

Therefore $\tilde{h}(t; L)$ is found to follow $L\mathcal{F}(x)$ during both the transient and steady-state phases, where $\mathcal{F}(x)$ is given by equation 10.

3.5 Pile Height as a Function of System Size

From Fig. 4, we find corrections to scaling due to sites and grains being discretised. As maximum gradient cannot be exceeded, these effects only decrease average gradient. Assuming these corrections to scaling are of the form

$$\langle h(t; L)\rangle_t = a_0 L(1 - a_1 L^{-\omega_1} + a_2 L^{-\omega_2} + \dots), \tag{11}$$

where $\langle h\rangle$ is time averaged pile height and a_i, ω_i are positive constants. To find the first term in the series, rearranging equation 11 as

$$\frac{\langle h(t; L)\rangle_t}{L} = a_0(1 - a_1 L^{-\omega_1}), \tag{12}$$

removes the leading order behaviour.

To quantify the corrections to scaling we can perform a multi-parameter curve fit using the Scipy Python package[3] of equation 12, which matches the processed data very well, Fig. 5 (B). This gives values of $a_0 = 1.742 \pm 0.003, a_1 = 0.189 \pm 0.004$ and $\omega_1 = 0.496 \pm 0.020$. Adding a_0 to Fig. 5 (B) we see that it is the asymptotic limit of the average gradient, as expected, and multiplying equation 12 by L we can plot the fit parameters against the original data, which matches the leading order behaviour very well, Fig. 5 (A).

This confirms our theoretical arguments in section 3.3 that for sufficiently large systems average gradient, a_0, is independent of system size.

3.6 Standard Deviation as a Function of System Size

Plotting the standard deviation of the time-averaged pile height, σ_h, against system length, we find that it follows a power law. By curve fitting a power law function to the data, we find σ_h scales with system length to the power 0.239 ± 0.001. Therefore σ_h scales slower than $\langle h\rangle$, meaning $\sigma_h/\langle h\rangle \to 0$ as $L \to \infty$.

3.7 Inter-Site Dependence

3.7.1 Considering Independent Sites

If site gradients were randomly distributed and independent from each other, then the mean gradient, and thus pile height, would follow the central limit theorem. Therefore we would expect pile height to have a Gaussian probability distribution of

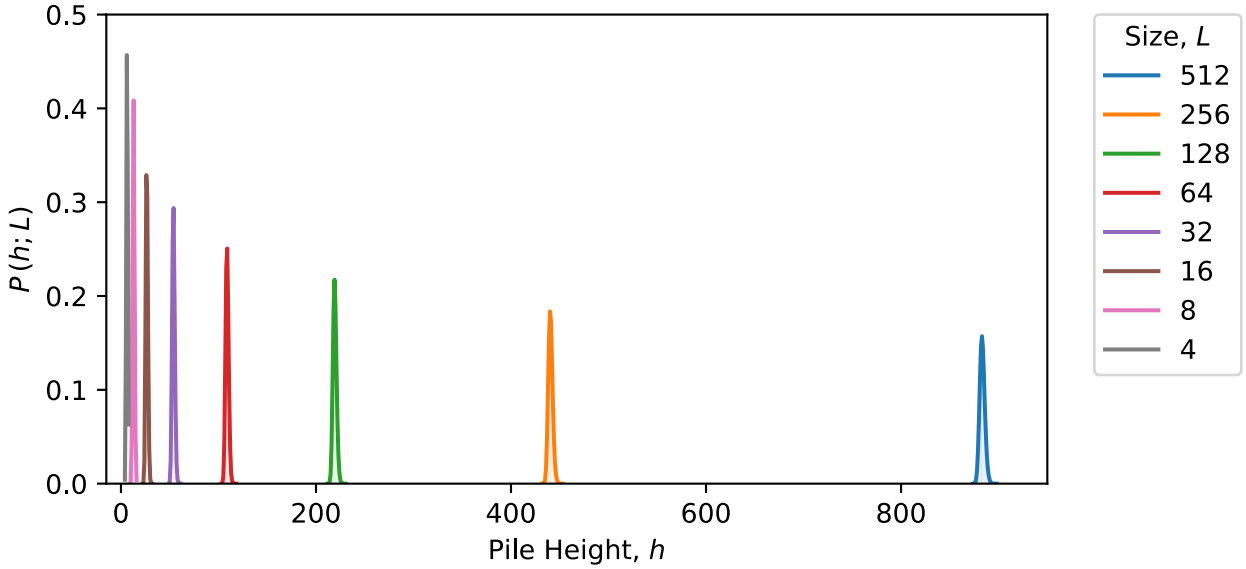

Figure 7: Normalised pile height probability distributions against pile height, for various system sizes. As expected, we find maximum probability density to decrease with increasing pile height, due to previous findings of increasing standard deviation on the mean pile height with increasing system size.

$$P(h;L) = \frac{1}{\sigma_h\sqrt{2\pi}} e^{-\frac{1}{2}\left(\frac{h-\langle h\rangle}{\sigma_h}\right)^2}, \tag{13}$$

with standard deviation

$$\sigma_h = L\frac{\sigma_z}{\sqrt{L}} = \sigma_z\sqrt{L}, \tag{14}$$

where σ_z is the standard deviation on the gradient of a single site, z_i. This disagrees with Fig. 6, since σ_h scales with system size to the power 0.239 ± 0.001, not 0.5, indicating the sites may not be independent.

3.7.2 Gaussian Data Collapse

For systems sizes between 4 and 512, we advance the system by L^2 time increments to ensure steady-state, as a maximum average gradient of 2 would require $1/2 \times L \times 2L = L^2$ grains to reach steady-state, before collecting pile height data for 1,000,000 further cycles. Plotting the normalised pile height probability distributions against pile height, Fig. 7, we find peak probability density to decrease with increasing pile height, as expected from increasing standard deviations, Fig. 6.

Rearranging equation 13 as

$$\sigma_h P(h;L) = \frac{1}{\sqrt{2\pi}} e^{-\frac{1}{2}\left(\frac{h-\langle h\rangle}{\sigma_h}\right)^2}, \tag{15}$$

we can plot $\sigma_h P$ against $\frac{h-\langle h\rangle}{\sigma_h}$ to collapse the data in Fig. 7 onto a single Gaussian of $\sigma = 1$ and $\langle h\rangle = 0$, Fig. 8 (A).

Investigating the quality of the data collapse shown in Fig. 8 (A), we can take the fractional difference between the data and the expected Gaussian from the central limit theorem, Fig. 8 (B). If the data followed the central limit theorem, this would show random and symmetric

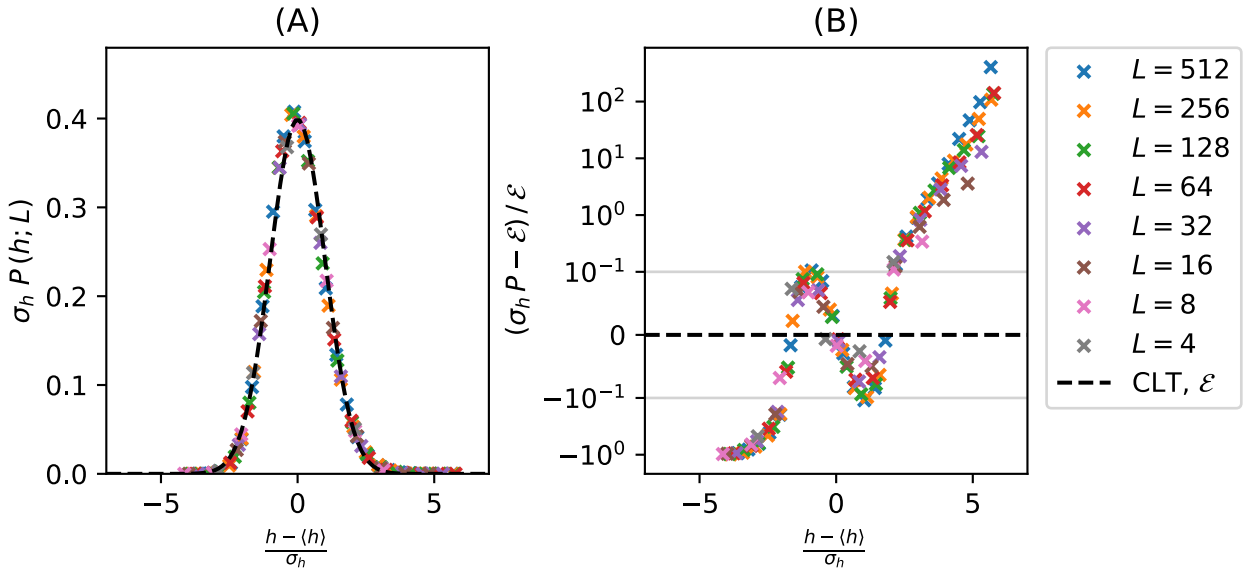

Figure 8: Collapsing the pile height probability distributions onto the the Gaussian expected by the central limit theorem (abreviated CLT) (A), and the fractional difference between the measured and expected (abreviated $\mathcal{E}$) values (B). Note the symmetric log axis on (B) with limits of ± 0.1, within which the graph becomes linear, marked by grey lines, to display negative values. The data clearly do not fall evenly about 0, instead showing the shifted mean and asymmetric tails characteristic of a normalised, positively skewed, Gaussian-like distribution.

noise about 0, for all scaled values of h. Instead, the tails are highly asymmetric, spanning many orders of magnitude. From the Gaussian derivative type oscillations about the origin, the peak of the distribution has been shifted towards negative h, as would be expected for the normalisation of a Gaussian-like distribution that has been positively skewed. The calculated skew of the collapsed data is found to be $+0.053$, which is positive as expected.

3.7.3 Implications

The positive skew observed in Fig. 8 in addition to the standard deviation on the mean pile height scaling as $L^{0.239\pm0.001}$ rather than $L^{0.5}$ in Fig. 6 are both strong evidence that the assumptions of the central limit theorem do not hold when applied to the Oslo model. Principally, the site gradients are not randomly distributed, independently of each other. This comes as no surprise, given that we specifically selected the Oslo model to investigate due to its rich complexity, which arises from interactions between sites.

Given interaction, we expect a smaller standard deviation on the mean pile height, as pile height is driven towards some value, given by some function of the nearby gradients. Similarly, given the presence of avalanches between sites we expect pile height to be positively skewed, due to the pile building up slowly but relaxing quickly, leading to an asymmetry in the amount of time spent at greater heights.

To corroborate our hypothesis of inter-site interactions, we would investigate the correlation length of the system, i.e. the typical length over which sites interact. Correlation is sufficient but not necessary to show interaction since it only indicates linear relationships. If correlation length were constant, then for large systems we would still expect the central limit theorem to apply as correlation length as a function of system length tends to zero. Therefore, to explain our previous findings, the correlation length would have to scale linearly with system size, since faster scaling would lead to the correlation length expanding beyond the system size, which is

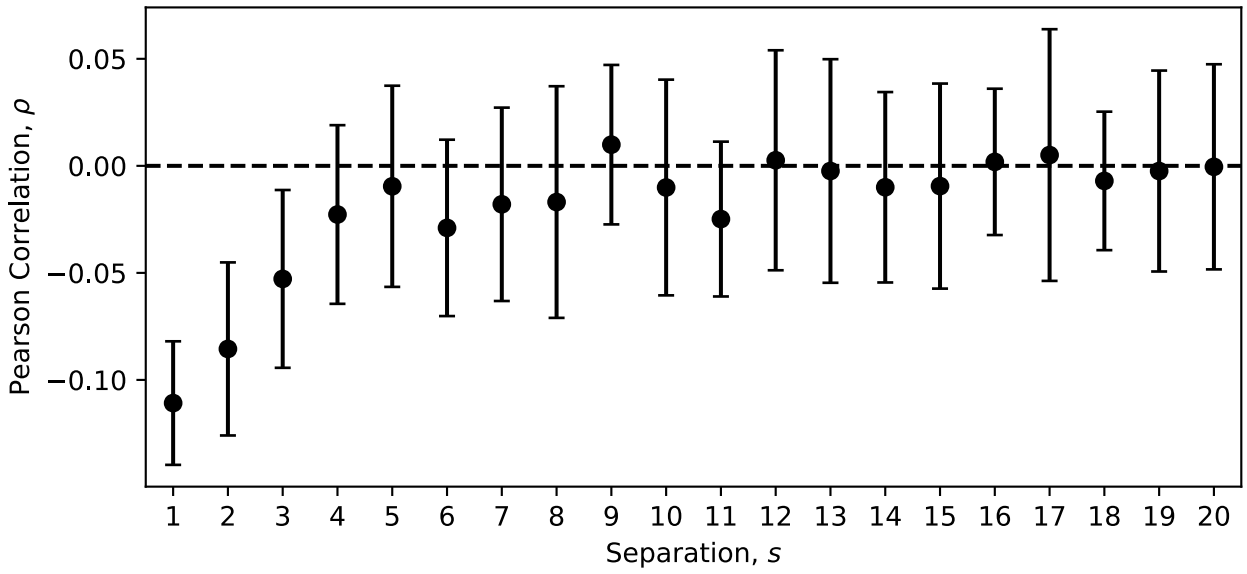

Figure 9: The Pearson product-moment correlation coefficient, ρ, between gradients of sites of a given separation, s, averaged over the $t = L^2$ gradients of 20 instances, for $L = 512$. Sites of separation 1 are adjacent, and non-zero correlation is observed between sites for separations less than 3.

non-physical.

Whilst finding the scaling relationship between the correlation length and the system size would require large amounts of high-quality data, finding any correlation between neighbouring sites is quite simple for a given system size. The Pearson correlation between steady-state gradients of sites of a given separation, for $L = 512$, Fig. 9, shows a negative correlation between the gradients of neighbouring sites, which decreases rapidly. Upon visual inspection, the correlation length is ≈ 3. The negative sign of the correlation likely arises from a relaxing site reducing its own gradient whilst increasing the gradients of the two adjacent sites.

4 Avalanche Size Investigation

Second, we investigate the probability distribution of avalanche sizes, with size given by the number of relaxations caused by the addition of a grain.

4.1 The Avalanche Size Probability Distribution

Recording avalanche size for 1,000,000 cycles after steady-state (L^2 cycles) gives the time series data in Fig. 10 (A). Logarithmic binning of the data, where each successive bin width was chosen to increase by a factor of 1.2, smooths out the noise generated by large sizes being sampled only a few times, using the provided log binning script by Max Falkenberg McGillivray. Plotting the binned probabilities, $\tilde{P}$, against s, Fig. 10 (B), we find a common scaling region, following some power law, followed by an L-dependent cut-off.

4.2 Finite Scaling Ansatz

We can ansatz that the probability follows a finite scaling function, of the form

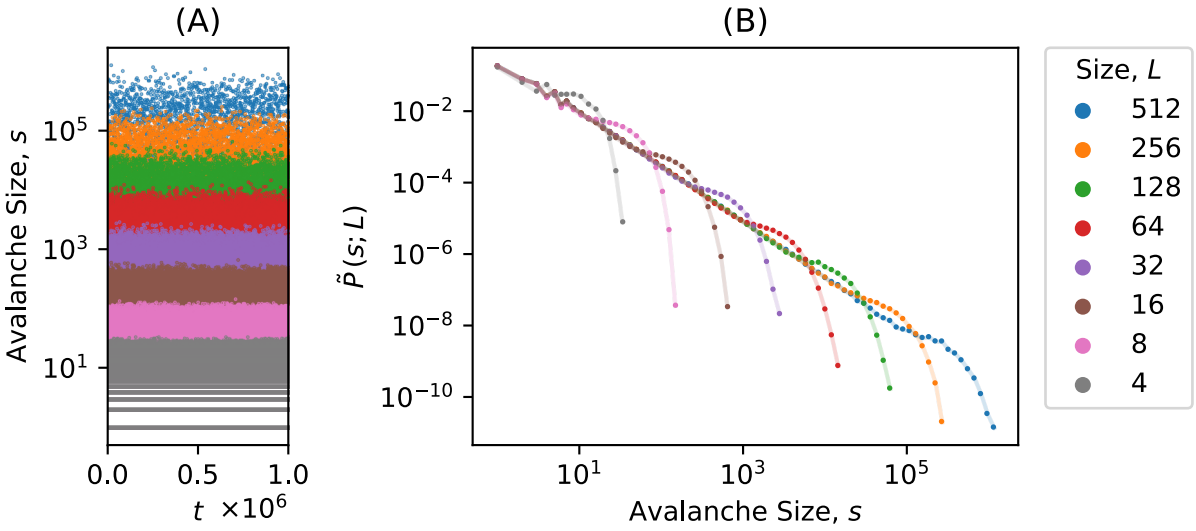

Figure 10: Avalanche size over time (A) and probability distribution of avalanche size against avalanche size on logarithmic axes (B) for various system sizes. Larger system sizes produce larger avalanches, with the probability distributions following a common scaling region following a power law, followed by an L-dependent cutoff.

$$\tilde{P}(s;L) \propto s^{-\tau_s}\mathcal{G}(s/L^D), \tag{16}$$

where τ_s is the avalanche-size exponent and D is the avalanche dimension. Rearranging as

$$s^{\tau_s}\tilde{P}(s;L) \propto \mathcal{G}(s/L^D), \tag{17}$$

allows us to collapse the probabilities onto $\mathcal{G}$ by plotting $s^{\tau_s}\tilde{P}$ against s/L^D, Fig. 11. Here, D and τ_s were adjusted manually to achieve the best data collapse, evaluated by eye, giving $\tau_s = 1.56 \pm 0.01$ and $D = 2.19 \pm 0.01$. As equation 16 is only valid for $L \gg 1, s \gg 1$, $L = 4$ and 8 were removed from Fig. 11, as they did not follow the data collapse. The quality of the data collapse for larger systems is very good, indicating that the finite scaling ansatz is valid. The data collapse breaks down for small s, as expected, due to corrections to scaling.

4.3 Distribution Moment Analysis

We can measure the moments of the avalanche size probability distribution, to get a second set of values for D and τ_s. We can find the scaling relation of the moments by using the finite scaling ansatz:

$$\langle s^k \rangle = \sum_{s=1}^{\infty} s^k P(s;L) \propto \sum_{s=1}^{\infty} s^{k-\tau_s}\mathcal{G}(s/L^D) \tag{18}$$

and assuming the main contributions to the sum are from large s:

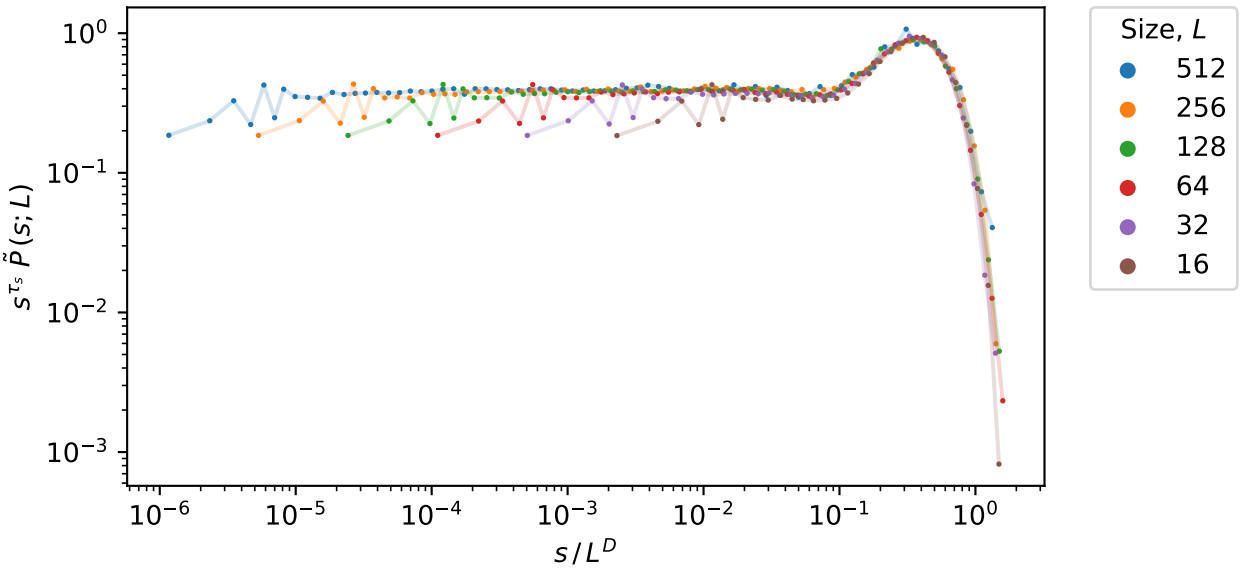

Figure 11: Collapsing the avalanche probabilities of various system sizes onto the scaling function proposed by the finite scaling ansatz. Sizes $L = 4$ and 8 are omitted, since the finite scaling ansatz is only valid for $L \gg 1$, and they do not lie on the same data collapse as the other system sizes. The collapse is of good quality, indicating the validity of the finite scaling ansatz equation for this system.

$$\langle s^k \rangle \propto \int_1^\infty s^{k-\tau_s} \mathcal{G}(s/L^D)\, ds \tag{19}$$

$$\text{let } u = \frac{s}{L^D} \tag{20}$$

$$\therefore\ du = \frac{1}{L^D} ds \tag{21}$$

$$\therefore\ \langle s^k \rangle \propto \int_{1/L^D}^\infty (L^D u)^{k-\tau_s} L^D \mathcal{G}(u)\, du \tag{22}$$

$$\propto L^{D(1+k-\tau_s)} \int_0^\infty u^{k-\tau_s} \mathcal{G}(u)\, du \tag{23}$$

$$\propto L^{D(1+k-\tau_s)}, \tag{24}$$

as the integral in equation 23 is independent of L for $L \gg 1$, and thus equals a constant if $1 + k - \tau_s > 0$ [1].

Measuring the moments of the data for various system sizes and fitting a power law, according to equation 24, allows us to find $D(1 + k - \tau_s)$, Fig. 12 (A). As this only holds for $L \gg 1$, $L = 4$ and 8 are omitted. Only the first 4 moments are taken, as higher moments give a greater weighting to large avalanches, which have fewer samples. We see that equation 24 is consistent with the data.

Fitting multiple moments allows us to plot $D(1 + k - \tau_s)$ against k, Fig. 12 (B), which is a linear relation with gradient D and y intercept $D(1 - \tau_s)$. This gives $D = 2.21 \pm 0.01$ and $\tau_s = 1.55 \pm 0.03$, which are very close to the values obtained from section 4.2, both lying within two standard deviations of each other.

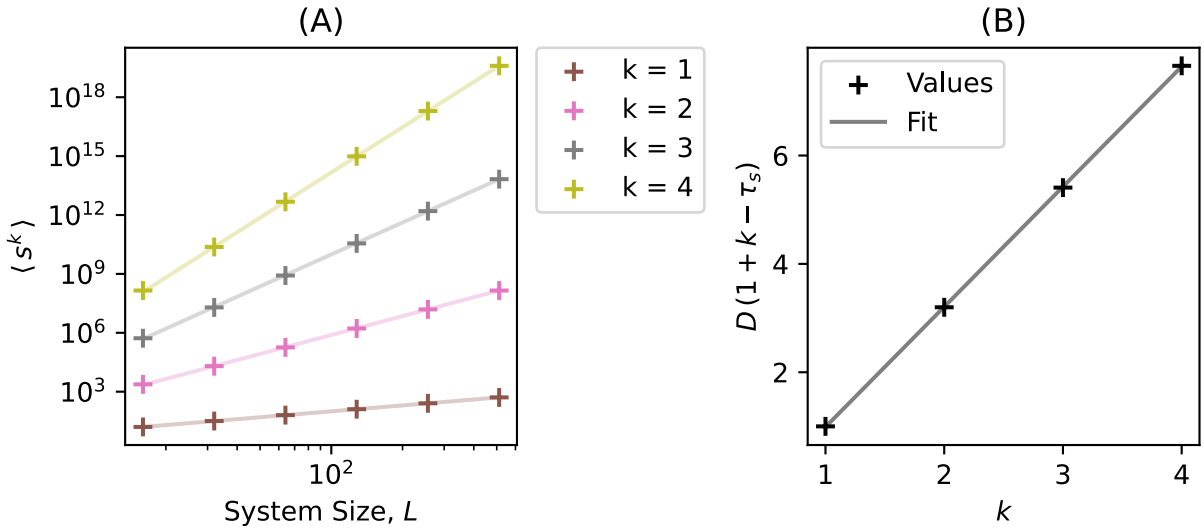

Figure 12: The first, second, third and fourth moments of s, against system size L, with each moment fitted to a power law (A) and the exponents of the resulting power laws for each moment, plotted against moment number, with linear regression to find the avalanche dimension D and the avalanche-size exponent τ_s (B). Errors have not been included in (B) as they would be too small to see, with values ranging from 2.6×10^{-3} for $k = 1$ to 2.7×10^{-4} for $k = 4$.

5 Conclusion

This study sought to investigate self-organised criticality through analysis of the Oslo model.

Pile height time series and cross-over times were analysed for various system sizes, together with a data collapse and subsequent corrections to scaling investigation. Basic theoretical scaling arguments were found to hold up well against empirical results, and by use of the central limit theorem, interactions were found to impact system dynamics. Follow up investigations into the scaling of correlation distance could build upon these results.

The probability distribution of avalanches was also investigated, with the finite scaling ansatz found to describe the distribution well. Large systems were found to produce a high quality data collapse and the avalanche dimension D and avalanche-size exponent τ_s were found to be 2.19 ± 0.01 and 1.56 ± 0.01 respectively from the data collapse, and from moment analysis 2.21 ± 0.01 and 1.55 ± 0.03, respectively, which are each within two standard deviations of the other, as expected. These results could be improved upon with larger data sets and system sizes.

Acknowledgements

The author would like to extend their gratitude to the two demonstrators and Professor Kim Christensen for their support throughout this investigation.

References

[1] K.Christensen and N.Maloney, *Complexity and Criticality*, Imperial College Press, London, 2005.

[2] P.Bak, C.Tang and K.Wiesenfeld *Self-organized criticality: An explanation of the 1/f noise*, American Physical Society 59 (1987).

[3] P.Virtanen, et al. *SciPy 1.0: Fundamental Algorithms for Scientific Computing in Python*, Nature Methods 17 (2020).